New paradigm for precision top physics: Weighing the top with energy correlators

Jack Holguin⊙,[1] Ian Moult,[2] Aditya Pathak⊙,[3] and Massimiliano Procura[4]

[1]*CPHT, CNRS, Ecole polytechnique, IP Paris, F-91128 Palaiseau, France*
[2]*Department of Physics, Yale University, New Haven, Connecticut 06511, USA*
[3]*University of Manchester, School of Physics and Astronomy, Manchester, M13 9PL, United Kingdom*
[4]*University of Vienna, Faculty of Physics, Boltzmanngasse 5, A-1090 Vienna, Austria*

Final states in collider experiments are characterized by correlation functions, $\langle \mathcal{E}(\vec{n}_1) \cdots \mathcal{E}(\vec{n}_k) \rangle$, of the energy flow operator $\mathcal{E}(\vec{n}_i)$. We show that the top quark imprints itself as a peak in the three-point correlator at an angle $\zeta \sim m_t^2/p_T^2$, with m_t the top quark mass and p_T its transverse momentum, providing access to one of the most important parameters of the Standard Model in one of the simplest field theoretical observables. Our analysis provides the first step toward a new paradigm for a precise top-mass determination that is, for the first time, highly insensitive to soft physics and underlying event contamination whilst remaining directly calculable from the Standard Model Lagrangian.

I. INTRODUCTION

The Higgs and top quark masses play a central role both in determining the structure of the electroweak vacuum [1–3], and in the consistency of precision Standard Model fits [4,5]. Indeed, the near criticality of the electroweak vacuum may be one of the most important clues from the Large Hadron Collider (LHC) for the nature of beyond the Standard Model physics [2,6–10]. This provides strong motivation for improving the precision of Higgs and top mass measurements.

While the measurement of the Higgs mass is conceptually straightforward both theoretically and experimentally [11], this could not be further from the case for the top mass (m_t). Due to its strongly interacting nature, a field theoretic definition of m_t, and its relation to experimental measurements, is subtle. In e^+e^- colliders, precision m_t measurements can be made from the threshold line shape [12–19]. However, this approach is not possible at hadron colliders, where, despite the fact that direct extractions have measured m_t to a remarkable accuracy [20–23], there is a debate on the theoretical interpretation of the measured "Monte Carlo (MC) top mass parameter" [24]. This has been argued to induce an additional $\mathcal{O}(1 \text{ GeV})$ theory uncertainty on m_t. For recent discussions, see [25,26]. It is therefore crucial to explore kinematic top-mass sensitive observables at the LHC where a direct comparison of the

experimental data with first principle theory predictions can be carried out.

Significant progress has been made in this regard from multiple directions. A unique feature of the LHC is that large numbers of top quarks are produced with sufficient boosts that they decay into single collimated jets on which jet shapes can be measured. In [27,28] it was shown using effective field theories (SCET and bHQET) [29–38] that factorization theorems can be derived for event shapes measured on boosted top quarks, enabling these observables to be expressed in terms of m_t in a field theoretically a well-defined field theoretic mass scheme [39–46]. Additionally, there has been substantial progress in parton shower algorithms capable of accurately simulating QCD radiation in fully exclusive top quark decays [47–66]. In Ref. [67], the groomed [68,69] jet mass was proposed as a m_t sensitive observable, realizing the factorization based approach of [27,28]. For measurements, see [70,71]. While jet grooming significantly improves the robustness of the observable, the complicated residual nonperturbative corrections [72] continue to be limiting factors in achieving a precision competitive with direct measurements, thereby motivating the exploration of observables not reliant on grooming.

In recent years, there has been a program to rethink [73] jet substructure directly in terms of correlation functions, $\langle \mathcal{E}(\vec{n}_1) \cdots \mathcal{E}(\vec{n}_k) \rangle$, of the energy flow in a direction $\vec{n}$ [74–81], $\mathcal{E}(\vec{n})$, motivated by the original work in QCD [82–91] and recent revival in conformal field theories (CFTs) [78–81,92–99]. These correlators have a number of unique and remarkable properties. Most importantly for phenomenological applications, correlators are insensitive to soft radiation without the application of grooming.
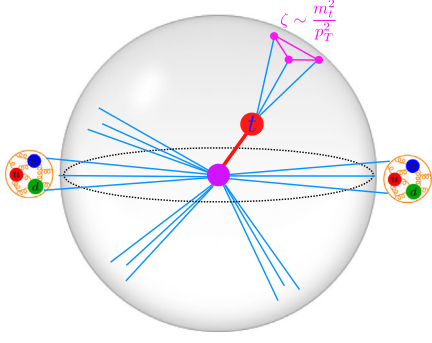
FIG. 1. A boosted top quark imprints its short lived existence onto the three-point correlator with a characteristic angle, $\zeta \sim (1 - \cos\theta)/2 \sim m_t^2/p_T^2$.

Additionally they can also be computed on tracks [73,100,101], using the formalism of track functions [102,103], allowing for higher angular resolution and suppressing pileup. However, so far their application has been restricted to massless quark or gluon jets [73,104–113].

In this paper, we present the first steps toward a new paradigm for precision m_t measurements based on the simple idea of exploiting the mass dependence of the characteristic opening *angle* of the decay products of the boosted top, $\zeta \sim m_t^2/p_T^2$ (see Fig. 1). The motivation for rephrasing the question in this manner is twofold. First, this angle can be accessed via low point correlators, which from a field theoretic point of view, is drastically more simple than a groomed substructure observable sensitive to ζ. Second, while the jet mass is sensitive to soft contamination and underlying event (UE), the angle ζ is not, since it is primarily determined by the hard dynamics of the top decay. In the following, we will present a numerical proof-of-principles analysis illustrating that the three-point correlator in the vicinity of $\zeta \sim m_t^2/p_T^2$ provides a simple, but highly sensitive probe of m_t, free of the typical challenges of jet-shape based approaches. Our goal is to provide the motivation for future precision studies and the motivation to find solutions to outstanding theoretical problems in the study of low point correlators.

II. THE THREE-POINT CORRELATOR

There has recently been significant progress in understanding the perturbative structure of correlation functions of energy flow operators. This includes the landmark calculation of the two-point correlator at next-to-leading order (NLO) in QCD [114,115] and next-to-next-to-leading order (NNLO) in $\mathcal{N} = 4$ super Yang-Mills [92,116], as well as the first calculation of a three-point correlator [105] at leading order (LO) (also further analyzed in [52,106,107]). The idea of using the three-point correlator to study the top quark is a natural one, and was considered early on in the jet substructure literature [117]. However, only due to this recent theoretical progress can we now make concrete steps toward a comprehensive program of

using energy correlators as a precision tool for Standard Model measurements [73,118].

The three-point correlator (EEEC) with generic energy weights is defined, following the notation in [105], as

$$G^{(n)}(\zeta_{12}, \zeta_{23}, \zeta_{31}) = \int d\sigma \widehat{\mathcal{M}}^{(n)}(\zeta_{12}, \zeta_{23}, \zeta_{31}), \quad (1)$$

with the measurement operator given by

$$
\begin{aligned}
&\widehat{\mathcal{M}}^{(n)}(\zeta_{12}, \zeta_{23}, \zeta_{31}) \\
&= \sum_{i,j,k} \frac{E_i^n E_j^n E_k^n}{Q^{3n}} \delta\left(\zeta_{12} - \hat{\zeta}_{ij}\right) \delta\left(\zeta_{23} - \hat{\zeta}_{ik}\right) \delta\left(\zeta_{31} - \hat{\zeta}_{jk}\right).
\end{aligned}
$$

(2)

Here $\hat{\zeta}_{ij} = (1 - \cos(\theta_{ij}))/2$, with θ_{ij} the angle between particles i and j, the sum runs over all triplets of particles in the jet, and Q denotes the hard scale in the measurement. The EEEC is not an event-by-event observable, but rather is defined as an ensemble average.

We are interested in the limit $\zeta_{12}, \zeta_{23}, \zeta_{31} \ll 1$, such that all directions of energy flow lie within a single jet. In the case of a CFT (or massless QCD up to the running coupling), the EEEC simplifies due to the rescaling symmetry along the lightlike direction defining the jet. In this case, the EEEC can be written in terms of a scaling variable, ζ_{31} and exhibits a featureless power-law scaling governed by the twist-2 spin-4 anomalous dimension, $\gamma(4)$ [78,96,104,105,107,119]. This behavior has been measured [118] using publicly released data from the CMS experiment data [120,121].

In contrast, m_t explicitly breaks the rescaling symmetry of the collinear limit. Thus m_t appears as a characteristic scale imprinted in the three-point correlator. While the top quark has a three-body decay at leading order, higher-order corrections give rise to additional radiation, which is primarily collinear to the decay products leading to a growth in the distribution at angles $\hat{\zeta}_{ij} \ll m_t^2/p_T^2$. To extract m_t, we therefore focus on the correlator in a specific energy flow configuration sensitive to the hard decay kinematics. Here we study the simplest configuration, that of an equilateral triangle $\hat{\zeta}_{ij} = \zeta$ allowing for a small asymmetry ($\delta\zeta$). Thus the key object of our analysis is the nth energy weighted cross section defined as

$$\frac{d\Sigma(\delta\zeta)}{dQ d\zeta} = \int d\zeta_{12} d\zeta_{23} d\zeta_{31} \int d\sigma \widehat{\mathcal{M}}_\triangle^{(n)}(\zeta_{12}, \zeta_{23}, \zeta_{31}, \zeta, \delta\zeta),$$

(3)

where the measurement operator $\widehat{\mathcal{M}}_\triangle^{(n)}$ is

$$
\begin{aligned}
&\widehat{\mathcal{M}}_\triangle^{(n)}(\zeta_{12}, \zeta_{23}, \zeta_{31}, \zeta, \delta\zeta) \\
&= \widehat{\mathcal{M}}^{(n)}(\zeta_{12}, \zeta_{23}, \zeta_{31}) \delta(3\zeta - \zeta_{12} - \zeta_{23} - \zeta_{31}) \\
&\quad \times \prod_{l,m,n \in \{1,2,3\}} \Theta(\delta\zeta - |\zeta_{lm} - \zeta_{mn}|).
\end{aligned}
$$

(4)

For $\delta\zeta \ll \zeta$,

$$\frac{d\Sigma}{d\zeta} \approx 4(\delta\zeta)^2 G^{(n)}(\zeta, \zeta, \zeta; m_t), \qquad (5)$$

where we have made the dependence on m_t explicit. Three-body kinematics implies that the distribution is peaked at $\zeta_{\text{peak}} \approx 3m_t^2/Q^2$, exhibiting quadratic sensitivity to m_t. At the LHC the peak is resilient to collinear radiation since $\ln\zeta_{\text{peak}} < 1/\alpha_s$, makings its properties computable in fixed order perturbation theory at the hard scale. In the region $\zeta < 2\delta\zeta$ the hard three-body kinematics is no longer identified, leading to a bulge in the distribution. In Fig. 2 we show these features in the simplest case of $e^+e^- \to t + X$ simulated using PYTHIA 8.3 parton shower, with the details of the simulation described below. We explain in Appendix A through a leading-order analysis how these features arise and motivate the definition of our observable stated above. Finally, we do not consider here the optimization of $\delta\zeta$ and leave it to future work.

III. MASS SENSITIVITY

To illustrate the mass sensitivity of our observable, we consider the simplest case of e^+e^- collisions simulated in PYTHIA 8.3 at a center of mass energy of $Q = 2000$ GeV using the PYTHIA 8.3 parton shower [122]. We reconstruct anti-k_T [123] jets with $R = 1.2$ using FASTJET [124], and analyze them using the jet analysis software JETLIB [125]. Although jet clustering is not required in e^+e^-, this analysis strategy is chosen to achieve maximal similarity with the case of hadron colliders. In Fig. 2 we show the distribution of the three-point correlator in the peak region, both with and without the effects of hadronization. Agreement of the peak position with the leading-order expectation is found, showing that the observed behavior is dictated by the hard decay of the top. In Fig. 2, linear ($n = 1$) and quadratic ($n = 2$) energy weightings are used; see eq. (2). The latter is not collinear safe, but the collinear IR divergences can be
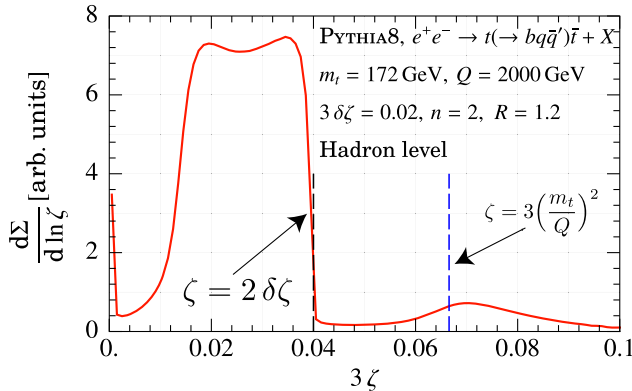

FIG. 2. Features of the EEEC measurement in equilateral triangle configuration on the tops.

absorbed into moments of the fragmentation functions or track functions [73,100].

Nonperturbative effects in energy correlators are governed by an additive underlying power law [76,90,91,126], which over the width of the peak has a minimal effect on the normalized distribution. This is confirmed by the small differences in peak position between parton and hadron level distributions. In Fig. 2 we also show an enlarged version for $n = 2$. Taking $m_t = 170, 172$ GeV with $n = 2$ as representative distributions, we find that the shift due to hadronization corresponds to a $\Delta m_t^{\text{Had}} \sim 250$ MeV shift in m_t. This is in contrast with the groomed jet mass case where hadronization causes peak shifts equivalent to $\Delta m_t^{\text{Had}} \sim 1$ GeV [67].

IV. HADRON COLLIDERS

We now extend our discussion to the more challenging case of proton-proton collisions. This study illustrates the difference between energy correlators and standard jet shape observables, and also emphasizes the irreducible difficulties of jet substructure at hadron colliders.

Implicit in the definition of energy correlators, $\langle\psi|\mathcal{E}(\vec{n}_1)\cdots\mathcal{E}(\vec{n}_k)|\psi\rangle$, is a characterization of the QCD final state $|\psi\rangle$. In the correlator literature, $|\psi\rangle$ is usually defined by a local operator of definite momentum acting on the QCD vacuum, $|\psi\rangle = \mathcal{O}|0\rangle$, giving rise to a perfectly specified hard scale, Q. This is the case of e^+e^- collisions. In hadronic final states at proton-proton collisions, the states on which we compute the energy correlators are necessarily defined through a measurement, e.g., by selecting anti-k_T jets with a specific $p_{T,\text{jet}}$. Due to the insensitivity of the energy correlators to soft radiation, we will show that it is in fact the nonperturbative effects on the jet p_T selection that are the only source of complications in a hadron collider environment. This represents a significant advantage of our approach, since it shifts the standard problem of characterizing nonperturbative corrections to infrared jet-shape observables, to characterizing nonperturbative effects on a *hard* scale. This enables us to propose a methodology for the precise extraction of m_t in hadron collisions by independently measuring the universal nonperturbative effects on the $p_{T,\text{jet}}$ spectrum. We now illustrate the key features of this approach.

The three-point correlator in hadron collisions is defined as

$$\widehat{\mathcal{M}}_{(pp)}^{(n)}(\zeta_{12}, \zeta_{23}, \zeta_{31})$$

$$= \sum_{i,j,k \in \text{jet}} \frac{(p_{T,i})^n (p_{T,j})^n (p_{T,k})^n}{(p_{T,\text{jet}})^{3n}}$$

$$\times \delta\left(\zeta_{12} - \hat{\zeta}_{ij}^{(pp)}\right)\delta\left(\zeta_{23} - \hat{\zeta}_{ik}^{(pp)}\right)\delta\left(\zeta_{31} - \hat{\zeta}_{jk}^{(pp)}\right), \qquad (6)$$

where $\hat{\zeta}_{ij}^{(pp)} = \Delta R_{ij}^2 = \sqrt{\Delta\eta_{ij}^2 + \Delta\phi_{ij}^2}$, with η, ϕ the standard rapidity, azimuth coordinates. The peak of the EEEC

distribution is determined by the hard kinematics and is found at $\zeta_{\text{peak}}^{(pp)} \approx 3m_t^2/p_{T,t}^2$, where $p_{T,t}$ is the hard top p_T, *not* $p_{T,\text{jet}}$.

To clearly illustrate the distinction between the infrared measurement of the EEEC and the hard measurement of the $p_{T,\text{jet}}$ spectrum, we present a two-step analysis using data generated in PYTHIA 8.3 (which we independently verified with VINCIA 2.3 [127]; see Fig. 7 below). First, we generated hard top quark states with definite momentum (like in e^+e^-), but in the more complicated LHC environment including UE, shown in Fig. 3, where we see a clear peak that is *completely*

FIG. 3. The $n = 1, 2$ three-point correlators on boosted tops in e^+e^- showing a clear peak at $\zeta \sim 3m_t^2/Q^2$. All graphs are normalized to peak height. The bottom plot shows an enlarged version of the $n = 2$ three-point correlator in e^+e^- for $m_t = 170$, 172 GeV, at both hadron and parton level. The dashed and solid lines are a polynomial fit to Monte Carlo data points.

independent of the presence of multi-parton interactions (MPI) (the PYTHIA 8.3 model for UE). This illustrates that the correlators themselves, on a perfectly characterized top quark state, are insensitive to soft radiation without grooming.

We then performed a proof-of-principles analysis to illustrate that a characterization of nonperturbative corrections to the $p_{T,\text{jet}}$ spectrum allows us to extract m_t, with small uncertainties from nonperturbative physics. While we will later give a factorization formula for the observable $d\Sigma(\delta\zeta)/dp_{T,\text{jet}}d\zeta$, for the present discussion it is useful to write it as

$$\frac{d\Sigma(\delta\zeta)}{dp_{T,\text{jet}}d\zeta} = \frac{d\Sigma(\delta\zeta)}{dp_{T,t}d\zeta}\frac{dp_{T,t}}{dp_{T,\text{jet}}}. \quad (7)$$

This formula, combined with Fig. 3, illustrates that the source of complications in the hadron-collider environment lies in the observable-independent function of *hard scales* $dp_{T,t}/dp_{T,\text{jet}}$, which receives both perturbative and nonperturbative contributions. To extract a value of m_t, we write the peak position as

$$\zeta_{\text{peak}}^{(pp)} = \frac{3F_{\text{pert}}(m_t, p_{T,\text{jet}}, \alpha_s, R)}{(p_{T,\text{jet}} + \Delta_{\text{NP}}(R) + \Delta_{\text{MPI}}(R))^2}. \quad (8)$$

Here F_{pert} incorporates the effects of perturbative radiation. At leading order, $F_{\text{pert}} = m_t^2$. Corrections from hadronization and MPI are encoded through the shifts $\Delta_{\text{NP}}(R)$ and $\Delta_{\text{MPI}}(R)$. Crucially, in the factorization limit that we consider, these are not a property of the EEEC observable, but can instead be extracted directly from the nonperturbative corrections to the jet p_T spectrum [128]. This is a unique feature of our approach.

To illustrate the feasibility of this procedure, we used PYTHIA 8.3 (including hadronization and MPI) to extract $\zeta_{\text{peak}}^{(pp)}$ as a function of $p_{T,\text{jet}}$, over an energy range within the expected reach of the high luminosity LHC. As a proxy for a perturbative calculation, we used parton level data to extract F_{pert}. To the accuracy we are working, F_{pert} is independent of the jet p_T, and can just be viewed as an effective top mass $\sqrt{F_{\text{pert}}}(m_t)$. We also extract $\Delta_{\text{NP}}(R) + \Delta_{\text{MPI}}(R)$ independently from the $p_{T,\text{jet}}$ spectrum. Note that an error of $\pm\delta$ on $\Delta_{\text{NP/MPI}}$ in a given $p_{T,\text{jet}}$ bin leads to an error on $\sqrt{F_{\text{pert}}}(m_t)$ of $\pm\delta\sqrt{F_{\text{pert}}}/p_{T,\text{jet}}$.

Using Eq. (6) we fit $\zeta_{\text{peak}}^{(pp)}$ as a function of $p_{T,\text{jet}}$ for an effective value of $F_{\text{pert}}(m_t)$. An example of the distribution in the peak region is shown in Fig. 4, which also highlights the insensitivity of the peak position to the use of charged particles only (tracks). A fit to $\zeta_{\text{peak}}^{(pp)}$ for several $p_{T,\text{jet}}$ bins is shown in Fig. 5. With a perfect characterization of the nonperturbative corrections to the EEEC observable, the value of $F_{\text{pert}}(m_t)$ extracted when hadronization and MPI
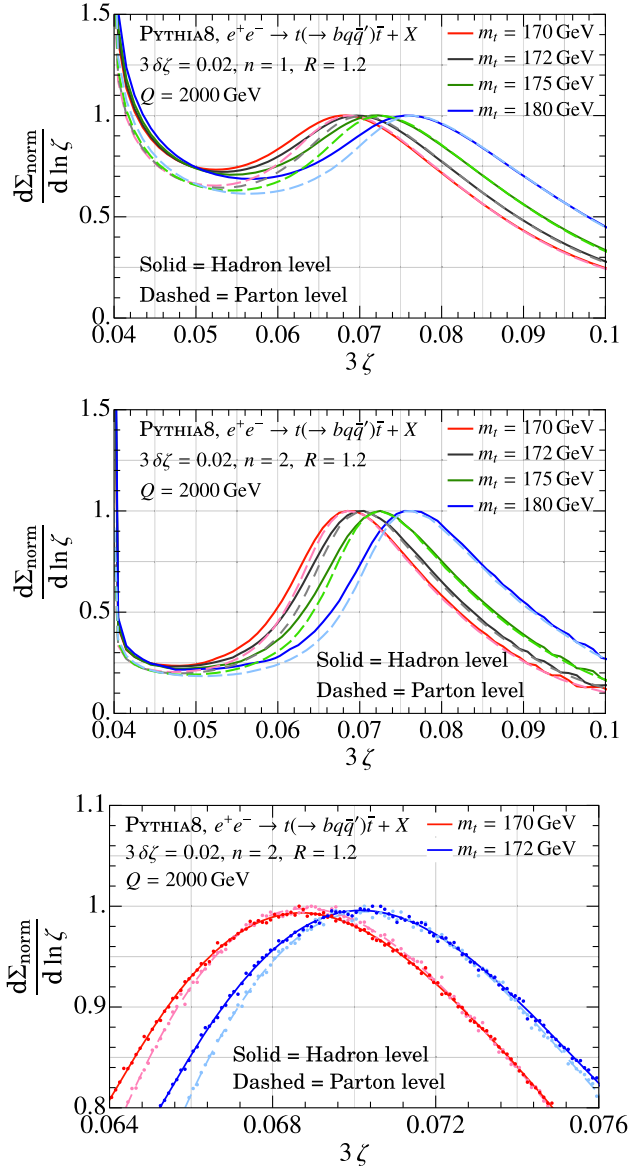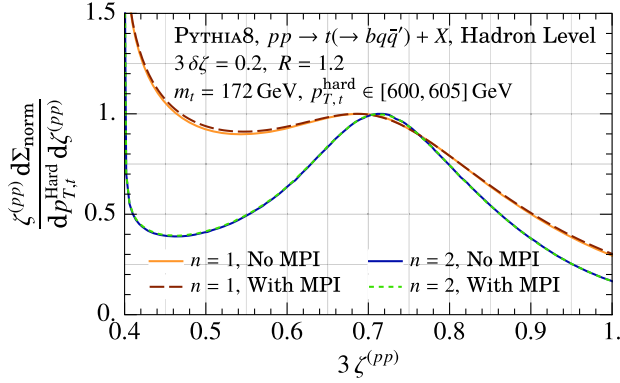
FIG. 4. The $n = 1, 2$ three-point correlators on decaying top quarks with a fixed hard p_T, with and without MPI. Here a clear peak can be seen at $\zeta \approx 3m_t^2/p_{T,t}^2$.

FIG. 6. Plot of the peak position as a function of $p_{T,\text{jet}}$, as used in our fitting procedure.

are included should exactly match its extraction at parton level. This would lead to complete control over m_t. In Table I we show the extracted value of $F_{\text{pert}}(m_t)$ from our parton level fit, and from our hadron + MPI level fit for two values of the PYTHIA 8.3 m_t. The errors quoted are the statistical errors on the parton shower analysis. The Hadron + MPI fit is quoted with two errors: the first originates from the statistical error on the EEEC measurement, and the second originates from the statistical error on the determination of $\Delta_{\text{NP}}(R) + \Delta_{\text{MPI}}(R)$ from the $p_{T,\text{jet}}$ spectrum. A more detailed discussion of this procedure is provided in Appendix B. Thus we find promising evidence that theoretical control of m_t, with conservative errors $\lesssim 1$ GeV, is possible with an EEEC-based measurement. Our analysis also emphasizes the importance of understanding nonperturbative corrections to the jet p_T spectrum. Theory errors are contingent upon currently unavailable NLO computations, discussed in the following section, and so are not provided. However, we expect

observable dependent NLO theory errors on m_t to be better than those in other inclusive measurements wherein in the dominant theory errors are from PDFs + α_s [129,130] and which mostly affect the normalization of the observable. By contrast the EEEC is also inclusive, but the extracted m_t is only sensitive to the observable's shape.

The goal of this paper has been to introduce our novel approach to top mass measurements, illustrating its theoretical feasibility and advantages. Our promising results motivate developing a deeper theoretical understanding of the three-point correlator of boosted tops in the hadron collider environment. Nevertheless, there remain many areas in which our methodology could be improved to achieve greater statistical power and bring it closer to experimental reality. These include the optimization of $\delta\zeta$, the binning of $p_{T,\text{jet}}$ and $\zeta^{(pp)}$, and including other shapes on the EEEC correlator. Regardless, our analysis does demonstrate the observable's potential for a precision m_t extraction when measured on a sufficiently large sample of boosted tops. We are optimistic that such a sample will be accessible at the high-luminosity LHC where it is forecast that $\sim 10^7$ boosted top events with $p_T > 500$ GeV will be measured [131].
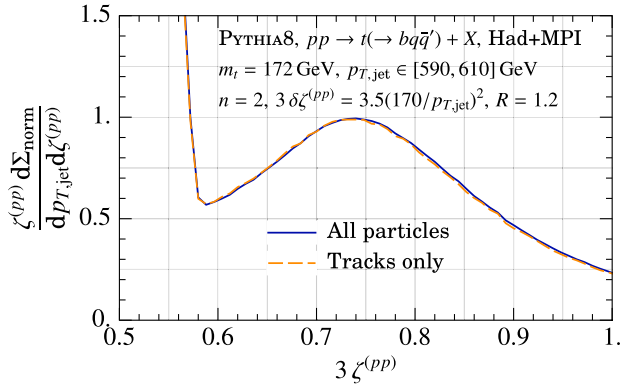

FIG. 5. The three-point correlator on top jets in hadron collisions. A clear peak can be seen at $\zeta \approx 3m_t^2/p_{T,\text{jet}}^2$ which is insensitive to the usage of tracks.
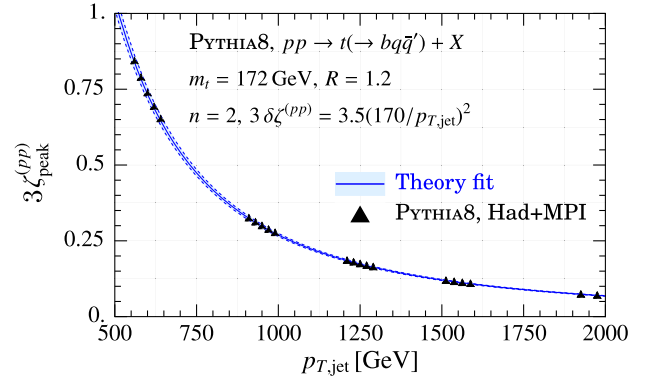
TABLE I. The effective parameter $F_{\text{pert}}(m_t)$ extracted at parton level, and hadron + MPI level. The consistency of the two simulations provides a measure of our uncertainty due to uncontrolled nonperturbative corrections. Statistical errors are shown.

PYTHIA 8.3 m_t	Parton $\sqrt{F_{\text{pert}}}$	Hadron + MPI $\sqrt{F_{\text{pert}}}$
172 GeV	172.6 ± 0.3 GeV	$172.3 \pm 0.2 \pm 0.4$ GeV
173 GeV	173.5 ± 0.3 GeV	$173.6 \pm 0.2 \pm 0.4$ GeV
175 GeV	175.5 ± 0.4 GeV	$175.1 \pm 0.3 \pm 0.4$ GeV
173–172	0.9 ± 0.4 GeV	1.3 ± 0.6 GeV
175–172	2.9 ± 0.5 GeV	2.8 ± 0.6 GeV

V. FACTORIZATION THEOREM

Combining factorization for massless energy correlators [132] with the bHQET treatment of the top quark near its mass shell [27,28,43,67] allows us to separate the dynamics at the scale of the hard production, the jet radius R, the angle ζ, and the top width Γ_t. While factorization is generically violated for hadronic jet shapes (see [133]), our framework is based on the rigorous factorization for single particle massive fragmentation [134–141]. Assuming $\zeta \ll R$, we perform a matching at the perturbative scale of the jet radius, using the fragmenting jet formalism [142–144], which captures the jet algorithm dependence. The final jet function describing the collinear dynamics at the scale of ζ is therefore free of any jet algorithm dependence. Correspondingly, we expect to obtain the following factorized expression,

$$\frac{\mathrm{d}\Sigma}{\mathrm{d}p_{T,\mathrm{jet}}\mathrm{d}\eta\,\mathrm{d}\zeta} = f_i \otimes f_j \otimes H_{i,j\to t}\left(z_J; p_{T,t} = \frac{p_{T,\mathrm{jet}}}{z_J}, \eta\right)$$
$$\otimes J_{t\to t}(z_J, z_h; R) \otimes J_{\mathrm{EEEC}}^{[\mathrm{tracks}]}(n, z_h, \zeta; m_t; \Gamma_t),$$
$$(9)$$

for the energy-weighted cross section differential in $p_{T,\mathrm{jet}}$, rapidity η, and ζ. This can be used to compute $F_{\mathrm{pert}}(m_t)$ in a systematically improvable fashion. Obvious dependencies, such as on factorization scales, have been suppressed for compactness. Here f_i are parton distribution functions, and $H_{i,j\to t}$ is the hard function for inclusive massive fragmentation [145,146], which is known for LHC processes at NNLO [147]. $J_{t\to t}$ is the fragmenting jet function, which is NLO for anti-k_T jets [143,144], but can be extended to NNLO using the approach of [148]. The convolutions over $f_{i,j}$ $H_{i,j\to t}$ and $J_{t\to t}$ alone determine the $p_{T,\mathrm{jet}}$ spectrum, independent of the EEEC measurement. Finally, J_{EEEC} is the energy correlator jet function, which can be computed in a well-defined short-distance top mass scheme (such as the MSR mass [39,41,149]), and can include information from track or fragmentation functions. Around the top peak, J_{EEEC} is almost entirely determined by perturbative physics and is currently known at LO. The NLO determination of J_{EEEC} is an outstanding theoretical problem and is very involved, thus beyond the scope of this paper, though a road map toward its completion has recently become available [105,114,115]. In the region of on shell top, J_{EEEC} can be matched onto a jet function defined in bHQET [27,28,39,40,67]. The functions in the factorization formula above exhibit standard DGLAP [150–152] evolution in the momentum fractions z_J and $z_h = p_{T,\mathrm{hadron}}/p_{T,\mathrm{jet}}$, and the $\otimes$ denote standard fragmentation convolutions. A more detailed study of the structure of the factorization will be provided in a future publication.

VI. CONCLUSIONS

We have proposed a new paradigm for jet-substructure based measurements of the top mass at the LHC in a rigorous field theoretic setup. Instead of using standard jet shape observables, we have analyzed the three-point correlator of energy flow operators, and have illustrated a number of its remarkable features. Our results support the possibility of achieving complete theoretical control over an observable with top mass sensitivity competitive with direct measurements whilst avoiding the ambiguities associated with the usage of MC event generators.

APPENDIX A: LEADING-ORDER ANALYSIS

Here we perform a leading-order analysis of the observable which suffices to explain the general features of the spectrum in Fig. 2. For concreteness, we will define the kinematics assuming a $e^+e^- \to t(\to bq\bar{q}') + X$ process where we take the $b, q, \bar{q}'$ partons to be massless. No further complications, beyond the need for more ink, are introduced by using the longitudinally invariant kinematics needed for measurements at the LHC. At leading order, we can factorize the Born cross section $\mathrm{d}\sigma^{(0)}/\sigma^{(0)}$ into the dimensionless three-body phase space for the top's decay products, $\mathrm{d}\Phi_3$, and the dimensionless weighted squared matrix element, $\sigma_t|M(t \to bW \to bq\bar{q}')|^2/\sigma^{(0)}$ where σ_t is the cross section to produce a top quark. As $|M(t \to bW \to bq\bar{q}')|^2 \sim \mathcal{O}(1)$, we can approximate the differential EEEC distribution in Eq. (3) as

$$\frac{1}{\sigma^{(0)}}\frac{\mathrm{d}\Sigma^{(0)}}{\mathrm{d}Q\mathrm{d}\zeta_{12}\mathrm{d}\zeta_{23}\mathrm{d}\zeta_{31}} \approx \int \mathrm{d}\Phi_3\,\widehat{\mathcal{M}}^{(n)}(\zeta_{12}, \zeta_{23}, \zeta_{31}), \quad (A1)$$

reducing the problem of understanding the observable of interest to studying three-body kinematics.

Before directly working with Eq. (A1), let us develop some intuition for the three-body kinematics. Consider the decay of a top quark in its rest frame, with $\tilde{p}_t = \tilde{p}_b + \tilde{p}_q + \tilde{p}_{\bar{q}'}$. Here we are using $\tilde{p}_i$ as a rest-frame momentum and p_i as a lab-frame momentum. In the top rest frame, the angular parameters on which the EEEC depends are given by

$$\tilde{\zeta}_{12} = \frac{\tilde{p}_b \cdot \tilde{p}_q}{2\tilde{E}_b \tilde{E}_q}, \qquad \tilde{\zeta}_{31} = \frac{\tilde{p}_b \cdot \tilde{p}_{\bar{q}'}}{2\tilde{E}_b \tilde{E}_{\bar{q}'}}, \qquad \tilde{\zeta}_{23} = \frac{\tilde{p}_q \cdot \tilde{p}_{\bar{q}'}}{2\tilde{E}_q \tilde{E}_{\bar{q}'}}.$$

$$(A2)$$

Momentum conservation requires that $\tilde{\zeta}_{12} + \tilde{\zeta}_{23} + \tilde{\zeta}_{31} \in [2, 2.25]$. Let the lab frame top momentum be $p_t = (E_t, \vec{p}_t)$. In the boost between the lab and rest frame, $\cosh\beta = E_t/m_t \sim \zeta^{-1/2}$. To first order in $m_t/E_t \ll 1$, we also have $\sinh\beta \approx \cosh\beta$. Hence the sum of lab frame EEEC parameters is

$$\zeta_{12} + \zeta_{23} + \zeta_{31}$$
$$\approx \left(\frac{m_t}{E_t}\right)^2 \left(\tilde{x}_{tb}\tilde{x}_{tq}\tilde{\zeta}_{12} + \tilde{x}_{tb}\tilde{x}_{t\bar{q}'}\tilde{\zeta}_{31} + \tilde{x}_{tq}\tilde{x}_{t\bar{q}'}\tilde{\zeta}_{23}\right), \quad (A3)$$

where

$$\tilde{x}_{ti} = (1 + \cos\tilde{\theta}_{ti}), \qquad (A4)$$

with $\tilde{\theta}_{ti}$ denoting the angle between parton i and the boost axis in the top's rest frame. The function

$$g \equiv \tilde{x}_{tb}\tilde{x}_{tq}\tilde{\zeta}_{12} + \tilde{x}_{tb}\tilde{x}_{t\bar{q}'}\tilde{\zeta}_{31} + \tilde{x}_{tq}\tilde{x}_{t\bar{q}'}\tilde{\zeta}_{23}$$

is also kinematically bounded so that $g \in [0, 3]$. Upon averaging over the possible boost axes one finds that $\langle g \rangle \in [1, 2.25]$. Thus, returning to Eq. (A1), we expect the partially integrated EEEC distribution

$$\frac{d\Sigma}{dQd\zeta} = \int d\zeta_{12}d\zeta_{23}d\zeta_{31}$$
$$\times \frac{d\Sigma^{(0)}}{dQd\zeta_{12}d\zeta_{23}d\zeta_{31}}\delta(3\zeta - \zeta_{12} - \zeta_{23} - \zeta_{31}), \quad (A5)$$

to be peaked around $\zeta \approx \langle g \rangle m_t^2/(3E_t^2) \approx 2m_t^2/(3E_t^2)$. However, this peak will have a large width [of the order of $3m_t^2/(4E_t^2)$], whose origin can be understood by interpreting the parameters $\tilde{x}_{ti} \in [0, 2]$ as three sources of (correlated) random noise in the shape of the flow of energy which "smears" the EEEC distribution. We can largely remove the noise by constraining the shape of the energy flow on the celestial sphere. This is most simply done by requiring that $\sqrt{\zeta_{ij}}$ approximately form the sides of an equilateral triangle ($\sqrt{\zeta_{ij}} \approx \sqrt{\zeta_{ik}}$). Consequently,

$$\tilde{x}_{tb}\tilde{x}_{tq}\tilde{\zeta}_{12} \approx \tilde{x}_{tb}\tilde{x}_{t\bar{q}'}\tilde{\zeta}_{31} \approx \tilde{x}_{tq}\tilde{x}_{t\bar{q}'}\tilde{\zeta}_{23}, \qquad (A6)$$

removing two of the noisy degrees of freedom from the distribution. Upon including this constraint, we find that $\langle g \rangle \approx 2.1$ with a small variance. This motivates us to introduce an EEEC distribution on equally spaced triplets of partons and allow for small asymmetries around this configuration governed by the parameter $\delta\zeta$:

$$\frac{d\Sigma(\delta\zeta)}{dQd\zeta} = \int d\zeta_{12}d\zeta_{23}d\zeta_{31} \int d\sigma \widehat{\mathcal{M}}_{\triangle}^{(n)}(\zeta_{12}, \zeta_{23}, \zeta_{31}, \zeta, \delta\zeta),$$

$$(A7)$$

where the operator $\widehat{\mathcal{M}}_{\triangle}^{(n)}$ in the collinear limit is

$$\widehat{\mathcal{M}}_{\triangle}^{(n)}(\zeta_{12}, \zeta_{23}, \zeta_{31}, \zeta, \delta\zeta)$$
$$= \sum_{i,j,k} \frac{E_i^n E_j^n E_k^n}{Q^{3n}} \delta\left(\zeta_{12} - \frac{\theta_{ij}^2}{4}\right)\delta\left(\zeta_{31} - \frac{\theta_{ik}^2}{4}\right)\delta\left(\zeta_{23} - \frac{\theta_{jk}^2}{4}\right)$$
$$\times \delta(3\zeta - \zeta_{12} - \zeta_{23} - \zeta_{31}) \prod_{l,m,n \in \{1,2,3\}} \Theta(\delta\zeta - |\zeta_{lm} - \zeta_{mn}|).$$

$$(A8)$$

As previously explained, three-body kinematics determines that this distribution is peaked at $\zeta_{\rm peak} \approx 3m_t^2/(4E_t^2) \sim m_t^2/Q^2$. Furthermore, at the LHC the peak should be resilient to collinear radiation since $\ln\zeta_{\rm peak} < 1/\alpha_s$.

We can now complete our leading-order discussion by computing the Born contribution to Eq. (A7). Expanding for $\delta\zeta \ll \zeta$, we obtain

$$\frac{d\Sigma^0(\delta\zeta)}{dQd\zeta} \propto (\delta\zeta)^2 \int_0^1 dz_1 dz_2 dz_3 \left(\frac{z_1 z_2 z_3}{8}\right)^n$$
$$\times \delta\left(\frac{m_t^2}{4E_t^2} - z_1 z_2\zeta - z_1 z_3\zeta - z_2 z_3\zeta\right)$$
$$\times \delta(1 - z_1 - z_2 - z_3)|M(t \to bW \to bq\bar{q}')|^2,$$

$$(A9)$$

where $z_1 = E_b/E_t$ and $z_2 = E_{\bar{q}'}/E_t$. The delta function causes the distribution to be sharply peaked at $\zeta = 3m_t^2/(4E_t^2)$. This matches the intuition we have developed from considering pure kinematics.

Looking at Eq. (3) to all orders in α_s, up to power corrections in $\delta\zeta$,

$$\frac{d\Sigma(\delta\zeta)}{dQd\zeta} = 4(\delta\zeta)^2 G^{(n)}(\zeta, \zeta, \zeta)\left(1 + \mathcal{O}\left(\frac{\delta\zeta}{\zeta}\right)\right), \quad (A10)$$

where the latter to leading order in $\delta\zeta \ll \zeta$ can be written as

$$4(\delta\zeta)^2 G^{(n)}(\zeta, \zeta, \zeta) = \frac{d\Sigma^0(\delta\zeta)}{dQd\zeta} + \mathcal{O}(\alpha_s), \quad (A11)$$

whilst in the region where $2\delta\zeta > \zeta$

$$\frac{\mathrm{d}\Sigma(\delta\zeta)}{\mathrm{d}Q\mathrm{d}\zeta} \approx \int \mathrm{d}\zeta_{12}\mathrm{d}\zeta_{23}\mathrm{d}\zeta_{31} G^{(n)}(\zeta_{12},\zeta_{23},\zeta_{31}). \quad (A12)$$

Figure 7 demonstrates that this dependence on $\delta\zeta$ is born out in simulation for e^+e^- and pp collisions. To conclude, our discussion motivates that an optimal choice of $\delta\zeta$ will be a function of Q that strikes a balance between statistics and constraining the three-body kinematics ($\delta\zeta_{\mathrm{optimal}} \approx \kappa\zeta_{\mathrm{peak}}/2$ for $\kappa \lesssim 1$). A more sophisticated analysis may also sum over several shapes of energy flow on the celestial sphere to increase statistics—perhaps allowing for smaller values of $\delta\zeta_{\mathrm{optimal}}$.

Finally, in Fig. 8 we show the top peak in the three-point correlator for $n = 2$ in $e^+e^- \to t + X$ simulations in VINCIA 2.3. We find the peak position almost in line with that of PYTHIA 8.3, justifying our earlier assumption that the features of the observable are largely determined by the fixed-order expansion in α_s.
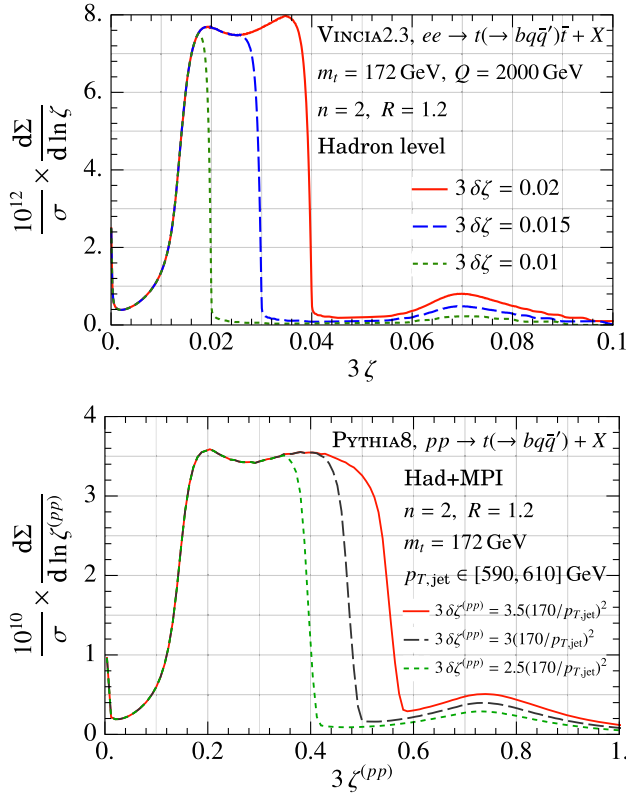

FIG. 7. The effect of applying different $\delta\zeta$ cuts to ensure an equilateral configuration for $e^+e^- \to t + X$ and $pp \to t + X$ processes. The $\delta\zeta$ cuts isolate the peak, which is governed by the hard decay of the top, from the "bulge" contribution.
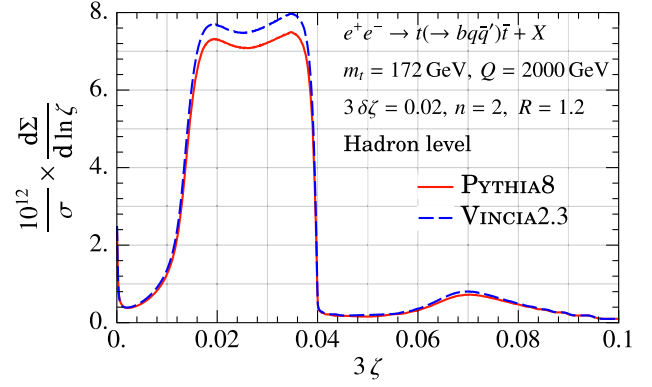

FIG. 8. Comparison of PYTHIA 8.3 and VINCIA 2.3 parton showers result. The differences in the peak positions are less than 300 MeV, and hence compatible with the uncertainties of our analysis.

APPENDIX B: DETAILS OF THE EEEC ANALYSIS AT HADRON COLLIDERS

Here we describe the details of the proof-of-principles peak position analysis outlined in Sec. IV. The longitudinal boost invariant measurement operator for the EEEC observable is

$$\widehat{\mathcal{M}}^{(n)}_{(pp)}(\zeta_{12},\zeta_{23},\zeta_{31})$$
$$= \sum_{i,j,k\in\mathrm{jet}} \frac{(p_{T,i})^n(p_{T,j})^n(p_{T,k})^n}{(p_{T,\mathrm{jet}})^{3n}}\delta\left(\zeta_{12}-\hat{\zeta}^{(pp)}_{ij}\right)$$
$$\times\delta\left(\zeta_{23}-\hat{\zeta}^{(pp)}_{ik}\right)\delta\left(\zeta_{31}-\hat{\zeta}^{(pp)}_{jk}\right), \quad (B1)$$

where $\hat{\zeta}^{(pp)}_{ij} = \Delta R^2_{ij} = \sqrt{\Delta\eta^2_{ij} + \Delta\phi^2_{ij}}$. As before, the peak of the $\widehat{\mathcal{M}}^{(n)}_{\triangle}$ EEEC distribution is determined by the top quark hard kinematics and is found at $\zeta^{(pp)}_{\mathrm{peak}} \approx 3m_t^2/p_{T,t}^2$, where $p_{T,t}$ is the hard top p_T, *not* $p_{T,\mathrm{jet}}$. Consequently, the basic properties of the $\mathrm{d}\Sigma(\delta\zeta)/\mathrm{d}p_{T,t}\mathrm{d}\zeta$ distribution are completely insensitive to nonperturbative physics. In Secs. III and IV we demonstrated this insensitivity by parton shower simulation wherein we showed evidence that the top decay peak is nearly entirely independent of hadronization and UE. Consequently, in the limit that $p_{T,t}/(\Delta_{\mathrm{NP}} + \Delta_{\mathrm{MPI}}) \to \infty$, the top decay peak position is exactly independent of nonperturbative effects. However, since $p_{T,t}$ is not directly accessible, the observable we consider is

$$\frac{\mathrm{d}\Sigma(\delta\zeta)}{\mathrm{d}p_{T,\mathrm{jet}}\mathrm{d}\zeta} = \frac{\mathrm{d}\Sigma(\delta\zeta)}{\mathrm{d}p_{T,t}\mathrm{d}\zeta}\frac{\mathrm{d}p_{T,t}}{\mathrm{d}p_{T,\mathrm{jet}}}, \quad (B2)$$

where $p_{T,\mathrm{jet}}$ is the p_T of an identified anti-k_T top jet. The top peak position in the distribution $\mathrm{d}\Sigma(\delta\zeta)/\mathrm{d}p_{T,\mathrm{jet}}\mathrm{d}\zeta$ will
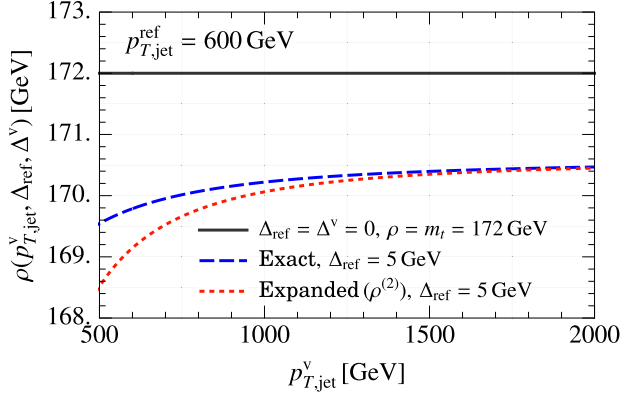
FIG. 9. The function ρ defined in Eq. (B5) for $\Delta^{\text{ref}} = 0$ GeV, as well as the exact and expanded to second order $(\rho^{(2)})$ for $\Delta^{\text{ref}} = 5$ GeV.

be shifted by hadronization and UE due to shifts in the jet p_T distribution. This shift can be measured independently from our observable and will be universal to all measurements of energy correlators on top quarks at the LHC.

We can parametrize the all-orders peak position in $d\Sigma(\delta\zeta)/dp_{T,\text{jet}}d\zeta$ as

$$\zeta_{\text{peak}}^{(pp)} = 3(1 + \mathcal{O}(\alpha_s))\frac{m_t^2}{f(p_{T,\text{jet}}, m_t, \alpha_s, \Lambda_{\text{QCD}})^2}$$

$$\equiv 3(1 + \mathcal{O}(\alpha_s))\frac{m_t^2}{(p_{T,\text{jet}} + \Delta(p_{T,\text{jet}}, m_t, \alpha_s, \Lambda_{\text{QCD}}))^2}.$$
$$(B3)$$

Mainly, Δ receives three additive contributions from perturbative radiation, hadronization, and from UE/MPI:

$$\Delta = \Delta_{\text{pert}} + \Delta_{\text{NP}} + \Delta_{\text{MPI}}. \quad (B4)$$

Some simple manipulations can be made so as to minimize the sensitivity to Δ in an extracted value of m_t. We define the following function of measurable and perturbatively calculable quantities,

$$\rho^2(\zeta_{\text{peak}}^{(pp)\text{v}}, p_{T,\text{jet}}^{\text{v}}) = \left(\zeta_{\text{peak}}^{(pp)\text{ref}} - \zeta_{\text{peak}}^{(pp)\text{v}}\right)$$
$$\times \left(\frac{3(1 + \mathcal{O}(\alpha_s))}{(p_{T,\text{jet}}^{\text{v}})^2} - \frac{3(1 + \mathcal{O}(\alpha_s))}{(p_{T,\text{jet}}^{\text{ref}})^2}\right)^{-1},$$
$$(B5)$$

where $\zeta_{\text{peak}}^{(pp)\text{ref}}$ is the peak position in a fixed reference p_T bin, $p_{T,\text{jet}}^{\text{ref}}$, and $\zeta_{\text{peak}}^{(pp)\text{v}}$ is the peak position for a variable $p_{T,\text{jet}}$ value, $p_{T,\text{jet}}^{\text{v}}$, larger than the reference value (we require $p_{T,\text{jet}}^{\text{v}} > p_{T,\text{jet}}^{\text{ref}}$ to avoid divergences). ρ^2 is defined so that, in the limit $p_{T,\text{jet}}^{\text{v}}, p_{T,\text{jet}}^{\text{ref}} \to \infty$, we have $\rho^2 \to m_t^2$. In the

analysis below we set $3(1 + \mathcal{O}(\alpha_s)) \mapsto 3$ so that, in the limit $p_{T,\text{jet}}^{\text{v}}, p_{T,\text{jet}}^{\text{ref}} \to \infty$, we find $\rho^2 \to F_{\text{pert}}$ as defined in Eq. (8). Now let us make a further definition,

$$\Delta^{\text{v}}(p_{T,\text{jet}}^{\text{v}} - p_{T,\text{jet}}^{\text{ref}}, m_t, \alpha_s, \Lambda_{\text{QCD}})$$
$$\equiv \Delta(p_{T,\text{jet}}^{\text{v}}, m_t, \alpha_s, \Lambda_{\text{QCD}}) - \Delta^{\text{ref}}, \quad (B6)$$

where

$$\Delta^{\text{ref}} \equiv \Delta(p_{T,\text{jet}}^{\text{ref}}, m_t, \alpha_s, \Lambda_{\text{QCD}}). \quad (B7)$$

We can substitute Eq. (B3) into Eq. (B5) to find $\rho(p_{T,\text{jet}}^{\text{v}}, \Delta^{\text{ref}}, \Delta^{\text{v}})$, which is plotted in Fig. 10, left.

ρ has an asymptote as $p_{T,\text{jet}}^{\text{v}} \to \infty$ around which we perform a series expansion:

$$\rho(p_{T,\text{jet}}^{\text{v}}, \Delta^{\text{ref}}, \Delta^{\text{v}})$$
$$= \sqrt{F_{\text{pert}}}\frac{p_{T,\text{jet}}^{\text{ref}}}{p_{T,\text{jet}}^{\text{ref}} + \Delta^{\text{ref}}}\left(1 - \frac{2p_{T,\text{jet}}^{\text{ref}}\Delta^{\text{ref}} + (\Delta^{\text{ref}})^2}{2(p_{T,\text{jet}}^{\text{v}})^2}\right.$$
$$\left. + \frac{(p_{T,\text{jet}}^{\text{ref}} + \Delta^{\text{ref}})^2(\Delta^{\text{ref}} + \Delta^{\text{v}})}{8(p_{T,\text{jet}}^{\text{v}})^3} + \mathcal{O}\left(\frac{1}{(p_{T,\text{jet}}^{\text{v}})^4}\right)\right). \quad (B8)$$

Thus a fit of the asymptote of ρ, and its first nonzero correction, can be used to extract F_{pert} and Δ^{ref}. All dependence on Δ^{v} enters in the higher-order terms. However, in the limit that $p_{T,\text{jet}}^{\text{ref}} \to \infty$, $\rho^2 \to F_{\text{pert}}$ and so while the fit for F_{pert} will become exact, the error on a fit for Δ^{ref} will diverge. In practice it will be necessary to perform the EEEC measurement with boosted tops in order to get a well-defined peak. Consequently, fits for Δ^{ref} will suffer from parametrically large errors (as can be seen in the large deviation between the exact and expanded curves at low

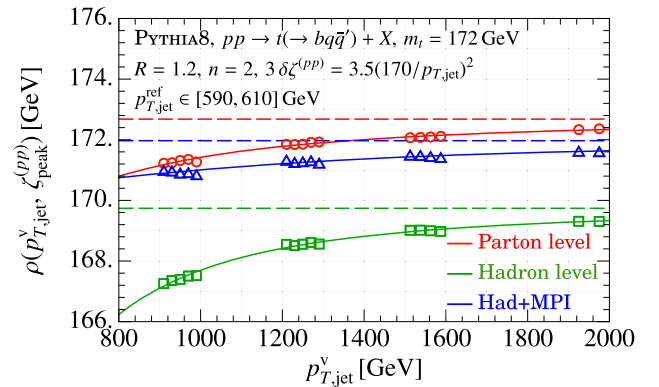FIG. 10. An example of the best fit for ρ's asymptote (ρ_{asy}) using the fit function in Eq. (B13). The data being fitted are produced using PYTHIA 8.3 with $m_t = 172$ and with $p_{T,\text{jet}}^{\text{ref}}$ binned in the range $p_{T,\text{jet}}^{\text{ref}} \in [590, 610]$ GeV. The dashed lines are the best fit for the asymptotes, $\rho = \rho_{\text{asy}}$.

TABLE II. A more detailed version of Table I, showing separate results at parton, hadron and hadron + MPI level. Five datasets for ρ were averaged over with $p_{T,\text{jet}}^{\text{ref}} \in [550, 650]$ GeV binned in 20 GeV intervals and $p_{T,\text{jet}}^{\text{v}} \in [900, 2000]$ GeV. One such dataset and its fit are shown in Fig. 10. In each column the first error is from the fit of the ρ asymptote and is statistical. The second error (when given) is also statistical and is the error from using the parton shower to determine $\Delta'^{\text{ref}} \approx \Delta^{\text{ref}}$ as extracted from the top jet p_t distribution. Errors have been combined in quadrature in the final row. No theory errors are given.

PYTHIA 8.3 m_t	EEEC Parton $\sqrt{F_{\text{pert}}}$	EEEC Hadron $\sqrt{F_{\text{pert}}}$	EEEC Hadron + MPI $\sqrt{F_{\text{pert}}}$
172 GeV	172.6 ± 0.3 GeV	$172.4 \pm 0.2 \pm 0.5$ GeV	$172.3 \pm 0.2 \pm 0.4$ GeV
173 GeV	173.5 ± 0.3 GeV	$173.9 \pm 0.3 \pm 0.5$ GeV	$173.6 \pm 0.2 \pm 0.4$ GeV
175 GeV	175.5 ± 0.4 GeV	$175.2 \pm 0.3 \pm 0.5$ GeV	$175.1 \pm 0.3 \pm 0.4$ GeV
173–172	0.9 ± 0.4 GeV	1.5 ± 0.8 GeV	1.3 ± 0.6 GeV
175–172	2.9 ± 0.5 GeV	2.8 ± 0.8 GeV	2.8 ± 0.6 GeV
175–173	2.0 ± 0.5 GeV	1.3 ± 0.8 GeV	1.5 ± 0.6 GeV

$p_{T,\text{jet}}^{\text{ref}}$ in Fig. 9). However, as previously stated, Δ^{ref} can be extracted from an independent measurement of the top-jet p_T distribution,

$$\frac{\mathrm{d}\sigma_{pp\to t(\to bq\bar{q}')+X}}{\mathrm{d}p_{T,\text{jet}}^{\text{ref}}} = D(m_t, p_{T,\text{jet}}, \alpha_s, \Lambda_{\text{QCD}}). \quad \text{(B9)}$$

One can parametrize the nonpertubative effects in D in the same way as we did in $\zeta_{\text{peak}}^{(pp)}$ to give

$$\begin{aligned} &D(m_t, p_{T,\text{jet}}, \alpha_s, \Lambda_{\text{QCD}}) \\ &= D^{\text{pert}}(m_t, g(p_{T,\text{jet}}, m_t, \alpha_s, \Lambda_{\text{QCD}}), \alpha_s), \end{aligned} \quad \text{(B10)}$$

where $D^{\text{pert}}(m_t, p_{T,\text{jet}}, \alpha_s)$ is the all-orders perturbative top-jet p_T distribution, and $g(p_{T,\text{jet}}, \ldots)$ captures all the nonperturbative modifications to $p_{T,\text{jet}}$. As before, we parametrize the modifications via introducing a shift function Δ' defined as

$$\Delta'(p_{T,\text{jet}}, m_t, \alpha_s, \Lambda_{\text{QCD}}) \equiv g(p_{T,\text{jet}}, m_t, \alpha_s, \Lambda_{\text{QCD}}) - p_{T,\text{jet}}, \quad \text{(B11)}$$

where

$$\Delta'^{\text{ref}} \equiv g(p_{T,\text{jet}}^{\text{ref}}, m_t, \alpha_s, \Lambda_{\text{QCD}}) - p_{T,\text{jet}}^{\text{ref}}. \quad \text{(B12)}$$

It is required for consistency with the factorization in Eq. (9) that, up to corrections which are suppressed by powers of $m_t/p_{T,\text{jet}}^{\text{ref}}$ and $\Lambda_{\text{QCD}}/p_{T,\text{jet}}^{\text{ref}}$, $\Delta'^{\text{ref}} \approx (\Delta^{\text{ref}} - \Delta_{\text{pert}}^{\text{ref}})$ where $\Delta_{\text{pert}}^{\text{ref}}$ is the perturbative contribution to Δ^{ref}. At the level of accuracy to which we are working, $\Delta_{\text{pert}}^{\text{ref}}$ can be absorbed into F_{pert} justifying why we dropped it above.

Thus, we fit for F_{pert} using the following procedure:

(i) Following Eq. (B8) we fit for the asymptote of ρ (which we label ρ_{asy}) using a polynomial in $(1/p_{T,\text{jet}}^{\text{v}})^n$. In this paper we found that a third degree polynomial,

$$\rho(p_{T,\text{jet}}) = \rho_{\text{asy}} + c_2(p_{T,\text{jet}}^{\text{v}})^{-2} + c_3(p_{T,\text{jet}}^{\text{v}})^{-3}, \quad \text{(B13)}$$
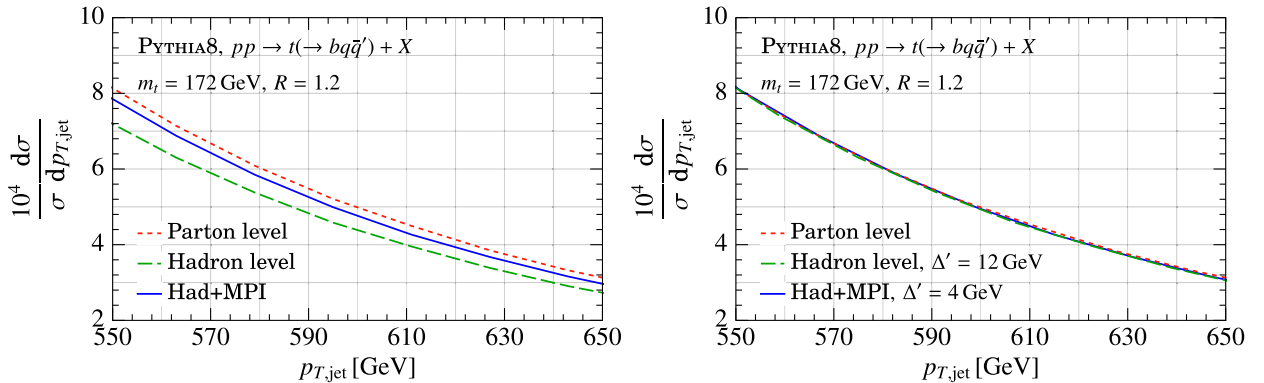

FIG. 11. On the left, the $p_{T,\text{jet}}$ spectrum at parton level, hadron level, and including MPI. A precise characterization of the states on which the energy correlator is computed requires an understanding of the nonperturbative shifts between these distributions. On the right, the hadron level and hadron + MPI curves shifted by constant values so that the three curves overlap. In both figures $p_{T,\text{jet}} \in [550, 650]$ GeV as this is the range in which we chose $p_{T,\text{jet}}^{\text{ref}}$ in our analysis.
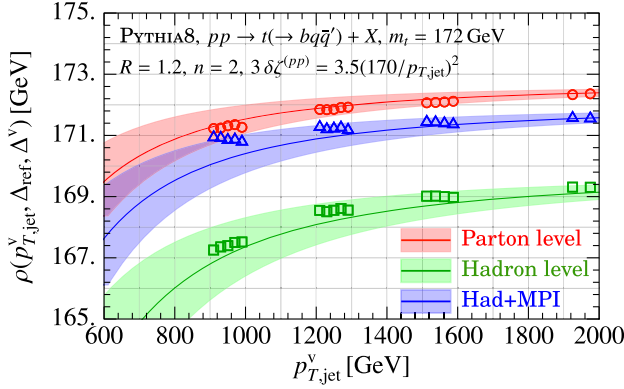
FIG. 12. This figure shows parton shower data for ρ generated in PYTHIA 8.3 at parton level, hadron level, and with MPI (shown in open markers) overlaid with curves from Eq. (B8) demonstrating the self-consistency of our results. Five datasets for ρ were averaged over with $p_{T,\mathrm{jet}}^{\mathrm{ref}} \in [550, 650]$ GeV binned in 20 GeV intervals.

optimized the reduced χ^2. The value of ρ_{asy} was found to be stable, within our statistical accuracy, against the inclusion of further higher-order terms, $c_n(p_{T,\mathrm{jet}}^{\mathrm{v}})^{-n}$. Figure 10 shows one such fit. No error bars are shown in Fig. 10 as it was produced from a single Monte Carlo sample. Fits of five samples are averaged over to produce the results and their errors in Table II.

(ii) We extract Δ'^{ref} from the top-jet p_T spectrum as shown in Fig. 11.

(iii) Finally, we compute F_{pert} using the asymptote of ρ, ρ_{asy}, defined above in Eq. (B13) as

$$\sqrt{F_{\mathrm{pert}}} = \rho_{\mathrm{asy}} \frac{p_{T,\mathrm{jet}}^{\mathrm{ref}} + \Delta^{\mathrm{ref}}}{p_{T,\mathrm{jet}}^{\mathrm{ref}}}. \qquad (\mathrm{B14})$$

The outcome of this procedure is given in Table II which shows the extracted F_{pert} from PYTHIA 8.3 with $m_t = 172$ GeV and 173 GeV. The important outcome of this analysis is that the differences between the measured masses with parton, hadron and hadron + MPI data are $\lesssim 1$ GeV and are smaller than the statistical errors. This analysis was not optimized to give a good statistical error and certainly can be improved. Thus we find promising evidence that complete theoretical control of the top mass, up to errors < 1 GeV, is possible with an EEEC based measurement.

To cross-check our result, purely to demonstrate self-consistency, in Fig. 12 we illustrate a theory fit of ρ using parton shower data from PYTHIA 8.3 with $m_t = 172$ GeV at parton level and hadron level. The curves in Fig. 12 are *not* the third degree polynomial used to extract ρ_{asy} in Eq. (B13). Rather, the curves are, truncated at second order, using the values of F_{pert} given in Table II and the values of Δ'^{ref} given in Fig. 11. Error bars correspond to the errors on F_{pert} and Δ^{ref}. To illustrate the partonic curve, a value of $\Delta_{\mathrm{pert}}^{\mathrm{ref}} = (11 \pm 3)$ GeV has been used which was extracted from the fit for $\rho^{(2)}$ [i.e., c_2 in Eq. (B13)]. This $\Delta_{\mathrm{pert}}^{\mathrm{ref}}$ is not used in any of the preceding analysis (or anywhere else in this article) where all dependence on $\Delta_{\mathrm{pert}}^{\mathrm{ref}}$ is absorbed into the definition of F_{pert}. Each error band shows the combined statistical error from the determination of the asymptote and of Δ^{ref} (including the dominant 3 GeV error on $\Delta_{\mathrm{pert}}^{\mathrm{ref}}$).

We find agreement between the MC data and our theory fit. Figure 13 along with Fig. 6 further demonstrates the excellent agreement between theory and parton shower data wherein we fit $\zeta_{\mathrm{peak}}(p_{t,\mathrm{jet}})$ with the ansatz in Eq. (8), also using the values for F_{pert} in Table II resultsmt and the values of Δ'^{ref} given in Fig. 11.
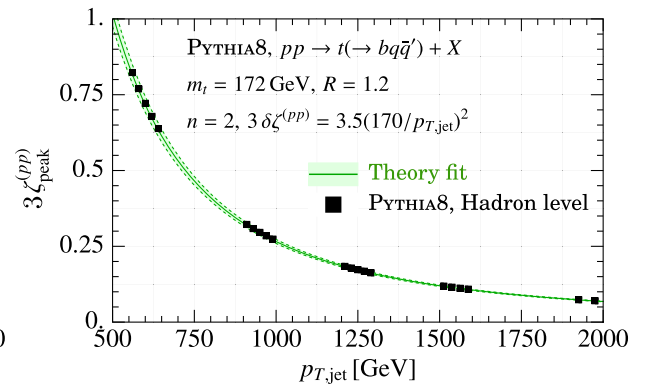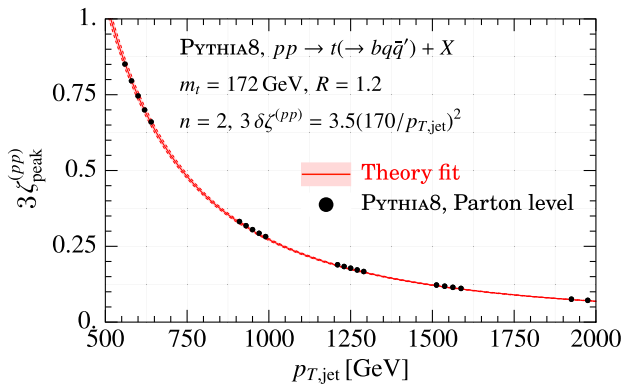

FIG. 13. Energy correlator peak positions as a function of $p_{T,\mathrm{jet}}$ at parton level and hadron level. (See Fig. 6 for an analogous figure including MPI). The theory fit uses the ansatz in Eq. (8) with the values of F_{pert} given in Table II and Δ'^{ref} extracted in Fig. 11. Excellent agreement between the theoretical fit and PYTHIA 8.3 is observed in all cases.

[1] G. Degrassi, S. Di Vita, J. Elias-Miro, J. R. Espinosa, G. F. Giudice, G. Isidori, and A. Strumia, J. High Energy Phys. 08 (2012) 098.

[2] D. Buttazzo, G. Degrassi, P. P. Giardino, G. F. Giudice, F. Sala, A. Salvio, and A. Strumia, J. High Energy Phys. 12 (2013) 089.

[3] A. Andreassen, W. Frost, and M. D. Schwartz, Phys. Rev. Lett. **113**, 241801 (2014).

[4] M. Baak, M. Goebel, J. Haller, A. Hoecker, D. Kennedy, R. Kogler, K. Moenig, M. Schott, and J. Stelzer, Eur. Phys. J. C **72**, 2205 (2012).

[5] M. Baak, J. Cúth, J. Haller, A. Hoecker, R. Kogler, K. Mönig, M. Schott, and J. Stelzer (Gfitter Group), Eur. Phys. J. C **74**, 3046 (2014).

[6] G. F. Giudice and R. Rattazzi, Nucl. Phys. **B757**, 19 (2006).

[7] J. Khoury and O. Parrikar, J. Cosmol. Astropart. Phys. 12 (2019) 014.

[8] J. Khoury, J. Cosmol. Astropart. Phys. 06 (2021) 009.

[9] G. Kartvelishvili, J. Khoury, and A. Sharma, J. Cosmol. Astropart. Phys. 02 (2021) 028.

[10] G. F. Giudice, M. McCullough, and T. You, J. High Energy Phys. 10 (2021) 093.

[11] G. Aad et al. (ATLAS, CMS Collaborations), Phys. Rev. Lett. **114**, 191803 (2015).

[12] V. S. Fadin and V. A. Khoze, JETP Lett. **46**, 525 (1987).

[13] V. S. Fadin and V. A. Khoze, Sov. J. Nucl. Phys. **48**, 309 (1988).

[14] M. J. Strassler and M. E. Peskin, Phys. Rev. D **43**, 1500 (1991).

[15] M. Beneke, Phys. Lett. B **434**, 115 (1998).

[16] M. Beneke, A. Signer, and V. A. Smirnov, Phys. Lett. B **454**, 137 (1999).

[17] A. H. Hoang, A. V. Manohar, I. W. Stewart, and T. Teubner, Phys. Rev. Lett. **86**, 1951 (2001).

[18] A. H. Hoang, A. V. Manohar, I. W. Stewart, and T. Teubner, Phys. Rev. D **65**, 014014 (2002).

[19] M. Beneke, Y. Kiyo, P. Marquard, A. Penin, J. Piclum, and M. Steinhauser, Phys. Rev. Lett. **115**, 192001 (2015).

[20] Tevatron Electroweak Working Group (CDF and D0 Collaborations), arXiv:1407.2682.

[21] V. Khachatryan et al. (CMS Collaboration), Phys. Rev. D **93**, 072004 (2016).

[22] M. Aaboud et al. (ATLAS Collaboration), Phys. Lett. B **761**, 350 (2016).

[23] P. A. Zyla et al. (Particle Data Group), Prog. Theor. Exp. Phys. **2020**, 083C01 (2020).

[24] A. H. Hoang and I. W. Stewart, Nucl. Phys. B, Proc. Suppl. **185**, 220 (2008).

[25] P. Nason, The Top Mass in Hadronic Collisions, in From My Vast Repertoire …: Guido Altarelli's Legacy, edited by A. Levy, S. Forte, and G. Ridolfi (World Scientific, Singapore, 2019), pp. 123–151.

[26] A. H. Hoang, Annu. Rev. Nucl. Part. Sci. **70**, 225 (2020).

[27] S. Fleming, A. H. Hoang, S. Mantry, and I. W. Stewart, Phys. Rev. D **77**, 114003 (2008).

[28] S. Fleming, A. H. Hoang, S. Mantry, and I. W. Stewart, Phys. Rev. D **77**, 074010 (2008).

[29] C. W. Bauer and I. W. Stewart, Phys. Lett. B **516**, 134 (2001).

[30] C. W. Bauer, S. Fleming, D. Pirjol, and I. W. Stewart, Phys. Rev. D **63**, 114020 (2001).

[31] C. W. Bauer, D. Pirjol, and I. W. Stewart, Phys. Rev. D **65**, 054022 (2002).

[32] C. W. Bauer, S. Fleming, D. Pirjol, I. Z. Rothstein, and I. W. Stewart, Phys. Rev. D **66**, 014017 (2002).

[33] E. Eichten and B. R. Hill, Phys. Lett. B **234**, 511 (1990).

[34] N. Isgur and M. B. Wise, Phys. Lett. B **232**, 113 (1989).

[35] N. Isgur and M. B. Wise, Phys. Lett. B **237**, 527 (1990).

[36] B. Grinstein, Nucl. Phys. **B339**, 253 (1990).

[37] H. Georgi, Phys. Lett. B **240**, 447 (1990).

[38] A. V. Manohar and M. B. Wise, Heavy quark physics, Vol. 10 (2000).

[39] A. H. Hoang, A. Jain, I. Scimemi, and I. W. Stewart, Phys. Rev. Lett. **101**, 151602 (2008).

[40] A. H. Hoang, A. Jain, I. Scimemi, and I. W. Stewart, Phys. Rev. D **82**, 011501 (2010).

[41] A. H. Hoang, A. Jain, C. Lepenik, V. Mateu, M. Preisser, I. Scimemi, and I. W. Stewart, J. High Energy Phys. 04 (2018) 003.

[42] A. H. Hoang, A. Pathak, P. Pietrulewicz, and I. W. Stewart, J. High Energy Phys. 12 (2015) 059.

[43] B. Bachu, A. H. Hoang, V. Mateu, A. Pathak, and I. W. Stewart, Phys. Rev. D **104**, 014026 (2021).

[44] M. Butenschoen, B. Dehnadi, A. H. Hoang, V. Mateu, M. Preisser, and I. W. Stewart, Phys. Rev. Lett. **117**, 232001 (2016).

[45] A. H. Hoang, S. Plätzer, and D. Samitz, J. High Energy Phys. 10 (2018) 200.

[46] ATLAS Collaboration, Report No. ATL-PHYS-PUB-2021-034, 2021.

[47] S. Höche, F. Krauss, and S. Prestel, J. High Energy Phys. 10 (2017) 093.

[48] S. Höche and S. Prestel, Phys. Rev. D **96**, 074017 (2017).

[49] F. Dulat, S. Höche, and S. Prestel, Phys. Rev. D **98**, 074013 (2018).

[50] M. Dasgupta, F. A. Dreyer, K. Hamilton, P. F. Monni, G. P. Salam, and G. Soyez, Phys. Rev. Lett. **125**, 052002 (2020).

[51] J. R. Forshaw, J. Holguin, and S. Plätzer, J. High Energy Phys. 09 (2020) 014.

[52] A. Karlberg, G. P. Salam, L. Scyboz, and R. Verheyen, Eur. Phys. J. C **81**, 681 (2021).

[53] K. Hamilton, R. Medves, G. P. Salam, L. Scyboz, and G. Soyez, J. High Energy Phys. 03 (2021) 041.

[54] J. Holguin, J. R. Forshaw, and S. Plätzer, Eur. Phys. J. C **81**, 364 (2021).

[55] Z. Nagy and D. E. Soper, Phys. Rev. D **104**, 054049 (2021).

[56] H. Brooks, C. T. Preuss, and P. Skands, J. High Energy Phys. 07 (2020) 032.

[57] K. Hamilton, A. Karlberg, G. P. Salam, L. Scyboz, and R. Verheyen, J. High Energy Phys. 03 (2022) 193.

[58] G. Bewick, S. Ferrario Ravasio, P. Richardson, and M. H. Seymour, J. High Energy Phys. 01 (2022) 026.

[59] L. Gellersen, S. Höche, and S. Prestel, Phys. Rev. D **105**, 114012 (2022).

[60] J. R. Forshaw, J. Holguin, and S. Plätzer, J. High Energy Phys. 05 (2022) 190.

[61] R. Frederix and S. Frixione, J. High Energy Phys. 12 (2012) 061.

[62] S. Hoeche, F. Krauss, P. Maierhoefer, S. Pozzorini, M. Schonherr, and F. Siegert, Phys. Lett. B **748,** 74 (2015).

[63] T. Ježo, J. M. Lindert, P. Nason, C. Oleari, and S. Pozzorini, Eur. Phys. J. C **76,** 691 (2016).

[64] R. Frederix, S. Frixione, A. S. Papanastasiou, S. Prestel, and P. Torrielli, J. High Energy Phys. 06 (2016) 027.

[65] K. Cormier, S. Plätzer, C. Reuschle, P. Richardson, and S. Webster, Eur. Phys. J. C **79,** 915 (2019).

[66] J. Mazzitelli, P. F. Monni, P. Nason, E. Re, M. Wiesemann, and G. Zanderighi, Phys. Rev. Lett. **127,** 062001 (2021).

[67] A. H. Hoang, S. Mantry, A. Pathak, and I. W. Stewart, Phys. Rev. D **100,** 074021 (2019).

[68] M. Dasgupta, A. Fregoso, S. Marzani, and G. P. Salam, J. High Energy Phys. 09 (2013) 029.

[69] A. J. Larkoski, S. Marzani, G. Soyez, and J. Thaler, J. High Energy Phys. 05 (2014) 146.

[70] A. M. Sirunyan et al. (CMS Collaboration), Eur. Phys. J. C **77,** 467 (2017).

[71] CMS Collaboration, Report No. CMS-PAS-TOP-19-005, 2019.

[72] A. H. Hoang, S. Mantry, A. Pathak, and I. W. Stewart, J. High Energy Phys. 12 (2019) 002.

[73] H. Chen, I. Moult, X. Zhang, and H. X. Zhu, Phys. Rev. D **102,** 054012 (2020).

[74] N. Sveshnikov and F. Tkachov, Phys. Lett. B **382,** 403 (1996).

[75] F. V. Tkachov, Int. J. Mod. Phys. A **12,** 5411 (1997).

[76] G. P. Korchemsky and G. F. Sterman, Nucl. Phys. **B555,** 335 (1999).

[77] C. W. Bauer, S. P. Fleming, C. Lee, and G. F. Sterman, Phys. Rev. D **78,** 034027 (2008).

[78] D. M. Hofman and J. Maldacena, J. High Energy Phys. 05 (2008) 012.

[79] A. Belitsky, S. Hohenegger, G. Korchemsky, E. Sokatchev, and A. Zhiboedov, Nucl. Phys. **B884,** 305 (2014).

[80] A. Belitsky, S. Hohenegger, G. Korchemsky, E. Sokatchev, and A. Zhiboedov, Nucl. Phys. **B884,** 206 (2014).

[81] P. Kravchuk and D. Simmons-Duffin, J. High Energy Phys. 11 (2018) 102.

[82] C. Basham, L. S. Brown, S. D. Ellis, and S. T. Love, Phys. Rev. Lett. **41,** 1585 (1978).

[83] C. L. Basham, L. S. Brown, S. D. Ellis, and S. T. Love, Phys. Rev. D **17,** 2298 (1978).

[84] C. L. Basham, L. S. Brown, S. D. Ellis, and S. T. Love, Phys. Lett. **85B,** 297 (1979).

[85] C. Basham, L. Brown, S. Ellis, and S. Love, Phys. Rev. D **19,** 2018 (1979).

[86] K. Konishi, A. Ukawa, and G. Veneziano, Nucl. Phys. **B157,** 45 (1979).

[87] F. V. Tkachov, Phys. Rev. Lett. **73,** 2405 (1994).

[88] F. V. Tkachov, Int. J. Mod. Phys. A **17,** 2783 (2002).

[89] D. Y. Grigoriev, E. Jankowski, and F. V. Tkachov, Phys. Rev. Lett. **91,** 061801 (2003).

[90] G. P. Korchemsky and G. F. Sterman, Nucl. Phys. **B437,** 415 (1995).

[91] G. P. Korchemsky, G. Oderda, and G. F. Sterman, AIP Conf. Proc. **407,** 988 (1997).

[92] A. Belitsky, S. Hohenegger, G. Korchemsky, E. Sokatchev, and A. Zhiboedov, Phys. Rev. Lett. **112,** 071601 (2014).

[93] A. Belitsky, S. Hohenegger, G. Korchemsky, and E. Sokatchev, Nucl. Phys. **B904,** 176 (2016).

[94] G. Korchemsky and E. Sokatchev, J. High Energy Phys. 12 (2015) 133.

[95] M. Kologlu, P. Kravchuk, D. Simmons-Duffin, and A. Zhiboedov, J. High Energy Phys. 11 (2020) 096.

[96] M. Kologlu, P. Kravchuk, D. Simmons-Duffin, and A. Zhiboedov, J. High Energy Phys. 01 (2021) 128.

[97] C.-H. Chang, M. Kologlu, P. Kravchuk, D. Simmons-Duffin, and A. Zhiboedov, J. High Energy Phys. 05 (2022) 059.

[98] G. Korchemsky, E. Sokatchev, and A. Zhiboedov, J. High Energy Phys. 08 (2022) 188.

[99] G. P. Korchemsky and A. Zhiboedov, J. High Energy Phys. 02 (2022) 140.

[100] Y. Li, I. Moult, S. S. van Velzen, W. J. Waalewijn, and H. X. Zhu, Phys. Rev. Lett. **128,** 182001 (2022).

[101] M. Jaarsma, Y. Li, I. Moult, W. Waalewijn, and H. X. Zhu, J. High Energy Phys. 06 (2022) 139.

[102] H.-M. Chang, M. Procura, J. Thaler, and W. J. Waalewijn, Phys. Rev. Lett. **111,** 102002 (2013).

[103] H.-M. Chang, M. Procura, J. Thaler, and W. J. Waalewijn, Phys. Rev. D **88,** 034030 (2013).

[104] L. J. Dixon, I. Moult, and H. X. Zhu, Phys. Rev. D **100,** 014009 (2019).

[105] H. Chen, M.-X. Luo, I. Moult, T.-Z. Yang, X. Zhang, and H. X. Zhu, J. High Energy Phys. 08 (2020) 028.

[106] H. Chen, I. Moult, and H. X. Zhu, Phys. Rev. Lett. **126,** 112003 (2021).

[107] H. Chen, I. Moult, and H. X. Zhu, J. High Energy Phys. 08 (2022) 233.

[108] I. Moult and H. X. Zhu, J. High Energy Phys. 08 (2018) 160.

[109] I. Moult, G. Vita, and K. Yan, J. High Energy Phys. 07 (2020) 005.

[110] A. Gao, H. T. Li, I. Moult, and H. X. Zhu, Phys. Rev. Lett. **123,** 062001 (2019).

[111] M. A. Ebert, B. Mistlberger, and G. Vita, J. High Energy Phys. 08 (2021) 022.

[112] H. T. Li, I. Vitev, and Y. J. Zhu, J. High Energy Phys. 11 (2020) 051.

[113] H. T. Li, Y. Makris, and I. Vitev, Phys. Rev. D **103,** 094005 (2021).

[114] L. J. Dixon, M.-X. Luo, V. Shtabovenko, T.-Z. Yang, and H. X. Zhu, Phys. Rev. Lett. **120,** 102001 (2018).

[115] M.-X. Luo, V. Shtabovenko, T.-Z. Yang, and H. X. Zhu, J. High Energy Phys. 06 (2019) 037.

[116] J. Henn, E. Sokatchev, K. Yan, and A. Zhiboedov, Phys. Rev. D **100,** 036010 (2019).

[117] M. Jankowiak and A. J. Larkoski, J. High Energy Phys. 06 (2011) 057.

[118] P. T. Komiske, I. Moult, J. Thaler, and H. X. Zhu, Phys. Rev. Lett. **130,** 051901 (2023).

[119] G. Korchemsky, J. High Energy Phys. 01 (2020) 008.

[120] S. Chatrchyan et al. (CMS Collaboration), J. Instrum. **3,** S08004 (2008).

[121] P. T. Komiske, R. Mastandrea, E. M. Metodiev, P. Naik, and J. Thaler, Phys. Rev. D **101**, 034009 (2020).

[122] T. Sjöstrand, S. Ask, J. R. Christiansen, R. Corke, N. Desai, P. Ilten, S. Mrenna, S. Prestel, C. O. Rasmussen, and P. Z. Skands, Comput. Phys. Commun. **191**, 159 (2015).

[123] M. Cacciari, G. P. Salam, and G. Soyez, J. High Energy Phys. 04 (2008) 063.

[124] M. Cacciari, G. P. Salam, and G. Soyez, Eur. Phys. J. C **72**, 1896 (2012).

[125] A. E. Ferdinand, A. Pathak *et al.* (to be published).

[126] A. V. Belitsky, G. P. Korchemsky, and G. F. Sterman, Phys. Lett. B **515**, 297 (2001).

[127] N. Fischer, S. Prestel, M. Ritzmann, and P. Skands, Eur. Phys. J. C **76**, 589 (2016).

[128] M. Dasgupta, L. Magnea, and G. P. Salam, J. High Energy Phys. 02 (2008) 055.

[129] S. Chatrchyan *et al.* (CMS Collaboration), Phys. Lett. B **728**, 496 (2014); **738**, 526(E) (2014).

[130] A. M. Sirunyan *et al.* (CMS Collaboration), J. High Energy Phys. 09 (2017) 051.

[131] P. Azzi *et al.*, CERN Yellow Rep. Monogr. **7**, 1 (2019).

[132] I. Moult, F. Ringer, and H. X. Zhu.

[133] J. R. Forshaw and J. Holguin, J. High Energy Phys. 12 (2021) 084.

[134] J. C. Collins and G. F. Sterman, Nucl. Phys. **B185**, 172 (1981).

[135] G. T. Bodwin, Phys. Rev. D **31**, 2616 (1985); **34**, 3932(E) (1986).

[136] J. C. Collins, D. E. Soper, and G. F. Sterman, Nucl. Phys. **B261**, 104 (1985).

[137] J. C. Collins, D. E. Soper, and G. F. Sterman, Nucl. Phys. **B308**, 833 (1988).

[138] J. C. Collins, D. E. Soper, and G. F. Sterman, Adv. Ser. Dir. High Energy Phys. **5**, 1 (1989).

[139] J. Collins, *Foundations of Perturbative QCD* (Cambridge University Press, Cambridge, England, 2013), Vol. 32.

[140] G. C. Nayak, J.-W. Qiu, and G. F. Sterman, Phys. Rev. D **72**, 114012 (2005).

[141] A. Mitov and G. Sterman, Phys. Rev. D **86**, 114038 (2012).

[142] M. Procura and I. W. Stewart, Phys. Rev. D **81**, 074009 (2010); **83**, 039902(E) (2011).

[143] Z.-B. Kang, F. Ringer, and I. Vitev, J. High Energy Phys. 10 (2016) 125.

[144] Z.-B. Kang, F. Ringer, and I. Vitev, J. High Energy Phys. 11 (2016) 155.

[145] B. Mele and P. Nason, Phys. Lett. B **245**, 635 (1990).

[146] B. Mele and P. Nason, Nucl. Phys. **B361**, 626 (1991); **B921**, 841(E) (2017).

[147] M. L. Czakon, T. Generet, A. Mitov, and R. Poncelet, J. High Energy Phys. 10 (2021) 216.

[148] H.-y. Liu, X. Liu, and S.-O. Moch, Phys. Rev. D **104**, 014016 (2021).

[149] A. H. Hoang, C. Lepenik, and M. Preisser, J. High Energy Phys. 09 (2017) 099.

[150] Y. L. Dokshitzer, Sov. Phys. JETP **46**, 641 (1977).

[151] V. N. Gribov and L. N. Lipatov, Sov. J. Nucl. Phys. **15**, 438 (1972).

[152] G. Altarelli and G. Parisi, Nucl. Phys. **B126**, 298 (1977).